New Method for Obtaining Palladium Particles on Y Zeolites. Characterization by TEM, ^{129}Xe NMR, H_2 Chemisorption, and EXAFS

David Guillemot, Michèle Polisset-Thfoin, and Jacques Fraissard*

Laboratoire de Chimie des Surfaces, CNRS URA 1428, Université Pierre et Marie Curie, case 196, 4 place Jussieu, T54-55, 75252 Paris, France

Dominique Bonnin

Laboratoire de Physique Quantique, CNRS URA 1428, ESCPI, 10, rue Vauquelin, 75005 Paris, France

Received: April 7, 1997; In Final Form: July 8, 1997[⊗]

Palladium particles on Y zeolites were prepared by a new method involving exchange of $[Pd(en)]^{2+}$ (en = ethylenediamine) with zeolite counterions and autoreduction of Pd(II) by the ligand in inert gas. An *in situ* extended X-ray absorption fine structure (EXAFS) experiment at the Pd K edge on a $[Pd(en)]^{2+}$/NaY sample shows reduction of Pd(II) to Pd(0) by the amine between 373 and 473 K. Pd/NaY and Pd/HY samples prepared by this method at 525 K were characterized by TEM, ^{129}Xe NMR, H_2 chemisorption, and EXAFS. These techniques were used to determine the local structure, size, and location of the Pd particles of freshly reduced samples (Pd/NaY, Pd/HY) and after heating in dioxygen at 573 K, followed by treatment with dihydrogen (Pd/NaYt, Pd/HYt). The TEM results show that the freshly reduced samples have particle sizes averaging 40 and 15 Å on NaY and HY zeolites, respectively. Treatment in dioxygen does not change particle sizes on HY zeolite but some large particles are seen on NaY zeolite. ^{129}Xe NMR results show that in freshly reduced samples the particles are surrounded by organic residues of the ligand which can be removed by dioxygen treatment. ^{129}Xe NMR and EXAFS results on samples without organic residues confirm that particles are smaller on Pd/HYt than on Pd/NaYt. Chemical anchoring of Pd clusters by zeolite H^+ is proposed to explain the different results for the zeolites. While H_2 chemisorption data on Pd/NaYt agree with other techniques, the amount of chemisorbed hydrogen on Pd/HYt disagrees completely with results of previous techniques, suggesting hydrogen suppression phenomena on the acid zeolite.

Introduction

Supported metals on zeolites are heterogeneous catalyst systems widely used in petrochemistry for conversion of heavy cuts (hydrocracking, hydroisomerization), transformation of light cuts (reforming, alkylation) and hydrogenation−dehydrogenation reactions.[1,2] Metal/zeolite systems are also useful for conversion of NO_x and CO, for example in commercial three-way exhaust catalysts.[3] Transition metals, particularly of the platinum group (Pt, Pd, etc.), are the most commonly used. In the hydrocarbon conversion processes, hydrogenation−dehydrogenation and isomerization sites are supplied by metals. In view of the cost of these metals and since metallic sites are progressively deactivated, by sintering, coking, and poisoning by sulfur and nitrogen compounds, improvements in the dispersion and stability are desirable.

For many years, supported palladium clusters have been studied intensively, owing to their importance in petroleum chemistry as the best catalysts for hydrogenation of olefins and for the hydrogenolysis of C−C, C−O, C−X, and C−N bonds, and palladium is the cheapest metal of the platinum group. For all these reasons it seemed crucial to find better conditions for preparing highly dispersed and stable palladium particles inside a zeolite framework. Unfortunately, while procedures for producing and stabilizing 10 Å platinum clusters in the NaY supercages have been known for a long time,[4] such procedures fail to provide 10 Å palladium clusters.[5] Effectively, if the usual genesis of palladium clusters inside faujasite cavities by cationic exchange of $Pd(NH_3)_4^{2+}$ and activation by high flow of pure O_2 at 473−573 K followed by reduction under H_2 below 420 K gives small palladium clusters in sodalite cages, subsequent heating over 623 K leads to the migration and agglomeration of primary particles into adjacent supercages. Many authors have proposed ways of avoiding the agglomeration of palladium in zeolites. Among these, Sachtler *et al.* showed that the introduction of Fe^{2+}, Mg^{2+}, or Ca^{2+} ions into NaY zeolite led to more stable palladium clusters.[6,7] More recently, original procedures using high-frequency ultrasonic[8] or organometallic chemical vapor deposition[9] led to small metallic palladium particles inside a zeolite framework, confirming the interest in the preparation of Pd/zeolite systems.

We recently reported[10] a method for preparing small stable gold particles located inside zeolite cavities by reduction of Au^{3+} by its ethylenediamine ligand in an inert gas. We showed that the acidity of Y zeolite has an important bearing on the size of the particles and their thermal stability. In view of these interesting results we have investigated the preparation of palladium particles in zeolite cavities using a similar procedure involving $[Pd(en)Cl_2]$ with NaY and H(Na)Y zeolites. Characterizations were carried out by TEM, ^{129}Xe NMR, EXAFS, and hydrogen chemisorption.

The ^{129}Xe NMR spectroscopy of adsorbed xenon was pioneered by Fraissard and co-workers[11] and has been widely used for the characterization of porous materials. At the same time, ^{129}Xe NMR was applied to the study of metal/zeolite systems and in recent years many authors have used this technique for investigating mono[12,13] and bimetallic[14] clusters, particularly Pt- and Pd-based systems, supported on zeolites. These studies confirmed that the chemical shift of the ^{129}Xe NMR spectrum was very sensitive to the location and the size

[⊗] Abstract published in *Advance ACS Abstracts,* September 1, 1997.

S1089-5647(97)01194-2 CCC: $14.00

TABLE 1: Samples, Reduction, Treatment, and Chemical Analysis

		% of elements (anhydrous zeolite)		
sample	treatment	Pd[a]	C	N
Pd/NaY	reduction inert flow 523 K	2.72	0.53	0.42
Pd/NaYt	reduction inert flow 523 K O_2 12 h 573 K, H_2 1 h 573 K	2.74	0.09	0.04
Pd/HY	reduction inert flow 523 K	2.92	0.75	1.20
Pd/HYt	reduction inert flow 523 K O_2 12 h 573 K, H_2 1 h 573 K	2.96	0.14	0.17

[a] Theoretical amount should be 3.1 wt % for zeolite without C and N.

of the metal clusters. In the present work, ^{129}Xe NMR spectroscopy was used to show the formation of palladium clusters inside zeolite cavities and to study their environment.

Experimental Section

1. Sample Preparation. Two types of catalysts (Table 1) were prepared from two industrial faujasites (LZY-54 and LZY-64) from UOP [NaY and NH_4(Na)Y, respectively, Si/Al = 2.7]. The NH_4(Na)Y zeolite was heated in a stream of inert gas (helium or argon) for 30 h with a slow rise in temperature (gradient: 12 K/h) up to 673 K and then held at this temperature for 10 h. In this way acid form H(Na)Y (elemental analysis: $H_{0.8}Na_{0.2}Y$, denoted HY) was obtained. Palladium was then introduced by ion exchange between the $[Pd(en)]^{2+}$ complex (en = ethylenediamine) and zeolite counterions. After solution of 285 mg of $[Pd(en)Cl_2]$ (Aldrich, 99%) in 400 mL of water, 5 g of zeolite was added so as to have 0.24 mmol of palladium per gram of zeolite (≈3.1 wt % of anhydrous zeolite). The mixture was stirred for 24 h at 333 K, filtered, and washed thoroughly with distilled water to eliminate chloride. After drying at room temperature (RT), samples were reduced in an inert atmosphere (helium, flow rate, 2 L/h), in a glass U-tube flow reactor, by raising the temperature linearly in 10 h from RT to 523 K and then maintaining this temperature for 12 h. After cooling under inert gas, the Pd/NaY and Pd/HY samples obtained were brown.

In order to eliminate carbon and nitrogen residues arising from oxidation of the ligand (en), both samples were treated with dioxygen for 12 h (6 L/h) at 573 K and then reduced again by H_2 for 1 h at the same temperature (denoted Pd/NaYt and Pd/HYt in Table 1).

Another $[Pd(en)]^{2+}$/NaY sample was reduced in inert gas in a controlled environment cell which allow *in situ* EXAFS measurements at various temperatures. This experiment was carried out at the Pd K edge to follow reduction of Pd(II) by the ligand with rise of temperature. The $[Pd(en)]^{2+}$/NaY sample was heated stepwise from RT to 573 K and cooled to RT for comparison with palladium foil at this temperature. EXAFS spectra were recorded at RT, 373 K, 473 K, 573 K, and RT again. Between two steps the temperature was increased at 480 K/h.

2. EXAFS Experiments. EXAFS measurements were carried out at beamline D 44 of LURE in the absorption mode at the Pd K edge using a Si(311) channel cut monochromator and gas ionization chambers. The monochromator was calibrated at the Pd K edge (24 352 eV) by recording an EXAFS spectrum of palladium foil. The X-ray energy was increased in 2.5 eV steps from 24 100 to 25 200 eV. The X-ray absorption data were analyzed by means of the XAFS computer program developed by Bonnin *et al.*[15]

For the determination of the structural parameters of palladium, Pd/NaYt and Pd/HYt samples were placed in the EXAFS sample holder (10 mm thick) with Kapton windows (Dupont, 125 μm); they were then examined in air at RT. The oscillating EXAFS function, $\chi(k)$, was extracted from the X-ray absorption spectra, normalized by the value of the absorption edge and weighted by k. The Fourier transform was applied between $k = 2.65$ and $k = 14.70$ Å^{-1} by using a Kaiser type window ($\tau = 3$). EXAFS oscillations from the first coordination shell were filtered by inverse Fourier transform between 1.17 and 3.37 Å, then fitted with the experimental phases/amplitudes of palladium foil and PdO powder.

3. Xenon Adsorption, ^{129}Xe NMR, and Hydrogen Chemisorption. Since the samples were stored without any particular precaution after reduction or after additional treatment, they were activated before any gas adsorption. Samples were evacuated (10^{-5} Torr) while the temperature was raised slowly (24 K/h) from RT to 573 K, then treated with 300 Torr of H_2 at 573 K for 1 h, and evacuated again at 673 K for 2 h.

Xenon adsorption and hydrogen chemisorption isotherms were determined at 300 K by means of a conventional volumetric gas adsorption apparatus. Xenon was adsorbed in the 1−600 Torr range. The ^{129}Xe NMR spectra were obtained with a 400 MHz MSL Brucker spectrometer operating at 110.64 MHz for ^{129}Xe; the repetition time was 1 s and the pulse duration 1 μs. The extrapolated shift of bulk xenon at zero density is used as reference for these measurements.

After xenon measurements, dihydrogen adsorption isotherms were performed to determine metal dispersion. Two adsorptions are carried out up to 20 Torr in order to avoid formation of a palladium hydride phase.[16] The first adsorption isotherm of dihydrogen corresponds to the total adsorbed dihydrogen. After evacuation at 300 K for about 30 min, the reversible physisorbed dihydrogen is removed. A second adsorption isotherm is then measured. The number of molecules irreversibly adsorbed at 300 K, corresponding to chemisorbed hydrogen, is given by the difference between the two straight lines extrapolated to zero pressure. Assuming a stoichiometry of one H atom per surface Pd atom,[17] we determined the metallic dispersion (D), defined as the percentage of metal atoms exposed at the surface of the particles.

4. Transmission Electron Microscopy (TEM). A Jeol JEM 100 CX II apparatus (3 Å resolution) was used. Samples were sectioned in order to check that the metal was inside the zeolite lattice. The embedding material was dissolved away to leave thin slices of the samples dispersed on a carbon TEM grid. The images, magnified 450 000 or 650 000 times, of the supported particles were used to determine the size distribution and the corresponding average diameter, and to check the homogeneity of particle distribution in the zeolite. Thermal treatment before hydrogen chemisorption and xenon adsorption measurements may lead to particle growth. TEM studies were, therefore, carried out after these experiments in order to get the best correlation between TEM particle sizes and dispersion calculated from hydrogen chemisorption.

Results and Discussion

The chemical analysis for palladium presented in Table 1 shows that the exchange between $[Pd(en)]^{2+}$ and the Na^+ or H^+ counterions of the zeolites is almost complete. The amounts of carbon and nitrogen for Pd/NaY and Pd/HY suggest that ethylenediamine is not easily removed during the reduction step. Although the amount of $[Pd(en)]^{2+}$ exchanged on the two zeolites is the same, the amounts of C and N are higher on HY, both before and after the additional step under O_2 at 573 K. However, this treatment leads to the elimination of about 80% of the carbon and 90% of the nitrogen (samples Pd/NaYt and Pd/HYt).

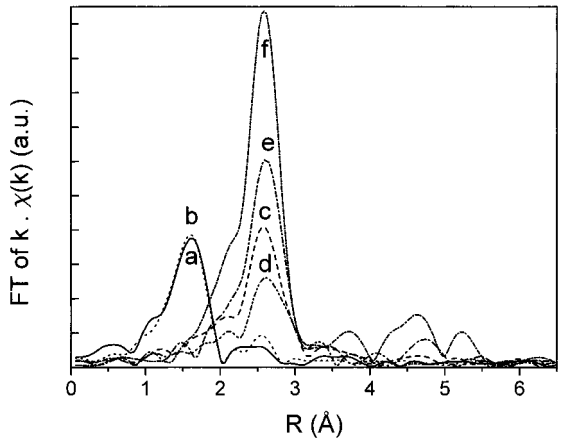

Figure 1. Radial structure functions of $[Pd(en)]^{2+}$/NaY in inert gas at RT (a), 373 K (b), 473 K (c), 573 K (d), cooled at RT (e) and Pd foil at RT (f). Pd K edge.

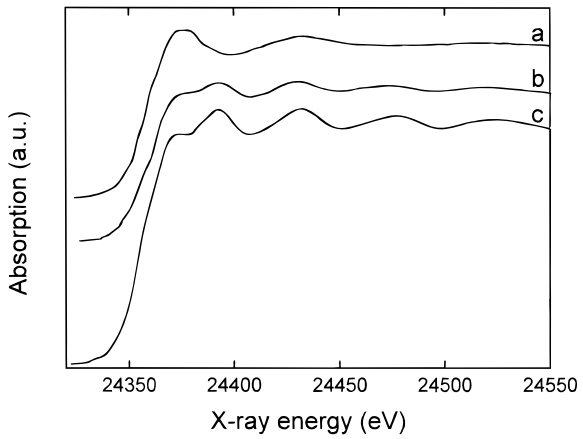

Figure 2. X-ray absorption spectra in the vicinity of Pd K absorption edge at RT: (a) $[Pd(en)]^{2+}$/NaY, (b) $[Pd(en)]^{2+}$/NaY heated under He at 573 K, (c) Pd foil.

1. Autoreduction of $[Pd(en)]^{2+}$ Complex Followed by *in situ* EXAFS. An *in situ* EXAFS experiment at the Pd K edge was carried out in order to follow the reduction of Pd(II) by its organic ligand in helium. In Figure 1 the Fourier transform (k weighted, $\Delta k = 2.65-14.70$ Å^{-1}) of EXAFS oscillations is plotted for various temperatures. Curve a is for the sample at RT before heating and curve b for the sample heated at 373 K, as described in the Experimental Section. They show one peak at about 1.6 Å (without phase correction) corresponding to light atoms in the first coordination shell of palladium.

Curve a cannot be fitted by assuming only the presence of nitrogen of the ligand in the first coordination shell of Pd(II). The better fit is obtained by considering N and O atoms in the first coordination shell of palladium with Pd−N and Pd−O distances equal to 1.99 and 2.07 Å, respectively. The number of nitrogen neighbors is fixed at 2.0, corresponding to one ligand around Pd(II). The Pd−N distance obtained is very close than the theoretical value reported for $[Pd(en)Cl_2]$.[18] The coordination number found for the oxygen neighbour is 1.81; this value agrees with the $[Pd(en)]^{2+}$ cation being near two $Z-O^-$ sites. The Fourier transform (curve a) is not affected by the increase in temperature to 373 K, which is a phenomenon characteristic of a well-organized structure. We consider, therefore, that the $[Pd(en)]^{2+}$ complex is not destroyed below 373 K and is coordinated in supercages with two $Z-O^-$ sites.

When the temperature is increased to 473 K the previous peak disappears completely and a new strong one appears at about 2.6 Å (curve c) as for palladium foil (curve f), corresponding to Pd(0) in the first coordination shell and, therefore, suggesting reduction of Pd(II) to Pd(0). If the temperature rises again to 573 K the intensity of the new peak decreases, probably because of increase in thermal disorder (curve d). After cooling to room temperature (curve e), the Fourier transform is similar to that of palladium foil but weaker.

Figure 2 displays the Pd K edge region of the EXAFS spectra of $[Pd(en)]^{2+}$ exchanged in zeolite (Figure 2a) and of the sample heated to 573 K and cooled to RT (Figure 2b) compared to that of palladium foil (Figure 2c). The adsorption edge resonance observed in curve a is characteristic of Pd(II). Pd(0) has no apparent edge resonance (curve c). The absorption edge spectra of $[Pd(en)]^{2+}$/NaY heated to 573 K (curve b) is similar to that of palladium foil, which confirms that palladium has been reduced to the zerovalent state. EXAFS oscillations of curve b are less intense than of curve c because the number of Pd(0) first neighbors in the supported sample is lower. In the same way, the intensity of the Pd(0)−Pd(0) contribution after cooling to RT is much lower than for metallic palladium foil (Figure 1, curves e and f), suggesting formation of nanoparticles despite the rapid temperature increase (480 K/h).

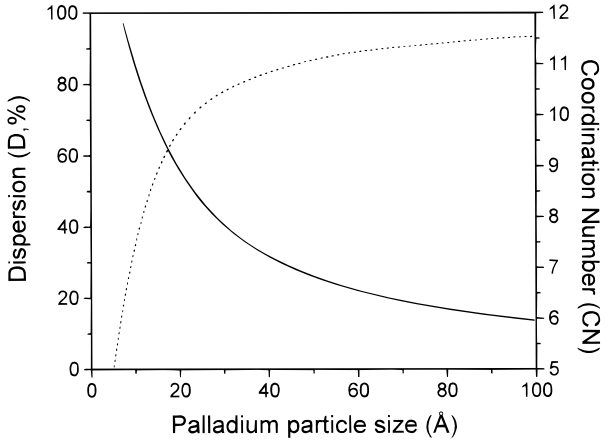

Figure 3. Correlation of palladium crystallite size with dispersion (—) or with average coordination number (···) assuming a fcc cubo-octahedron shape.

Finally, this *in situ* EXAFS experiment shows that Pd(II) can be reduced completely to Pd(0) by the ethylenediamine ligand, via the $[Pd(en)]^{2+}$ complex, between 373 and 473 K. This is not surprising, since the reduction of Pd(II) by amino groups has been known for a long time, for example by NH_3, in the case of $[Pd(NH_3)_4]^{2+}$.

2. Characterization of Samples Reduced under Mild Conditions. 2.1. Model for Particle Size Determination. TEM, hydrogen chemisorption, and EXAFS are three common techniques for obtaining information about the size of metallic particles in metal−zeolite systems. In order to compare these results we determined the average particle size through dispersion (D) and average coordination number (CN). Statistical calculations by Van Hardeveld and Hartog[19] give the average number of atoms per metallic particle (Nt) depending on D or CN and the assumed particle shape. The shape most commonly used for fcc transition metals is the cubo-octahedron. These authors showed also that the diameter of metallic particles (d) crystallizing in the fcc structure can be related to the average number of atoms per particle (Nt) by the relation $d = 1.105(\mathrm{Nt})^{1/3}d_{ato}$, where d_{ato} is the atomic diameter of the metal (2.76 Å for Pd).

From these considerations, Figure 3 represents the dependence of the palladium cluster size (d) on the metallic dispersion (D, %) or the average coordination number (CN) of palladium atoms

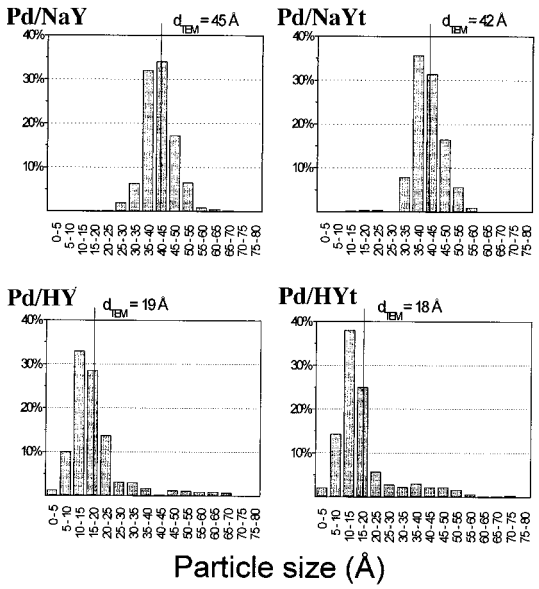

Figure 4. Particle size histograms of Pd/NaY, Pd/NaYt, Pd/HY, and Pd/HYt determined by TEM.

in the first coordination shell, assuming the fcc structure and that the crystallites are cubo-octahedral.

2.2. Transmission Electron Microscopy. In Figure 4 are presented the histograms of the particle size distribution determined by TEM for Pd/NaY and Pd/HY samples and for these two samples after additional treatment (Pd/NaYt, Pd/HYt). Average diameters d_{TEM} calculated from the histograms are reported in Table 2. The results show two distinct behaviors for the two zeolites used: on the NaY form the cluster size is homogeneously distributed around 40 Å (Pd/NaY, $d_{TEM} = 45$ Å), suggesting that during particle formation the NaY lattice is disrupted and partially destroyed in the vicinity of the palladium particles. Metallic particles (notably Pd, Ni, Ru, and Pt) larger than the dimensions of the supercages have often been observed by TEM in the lattice of NaY zeolite.[20] On the contrary, on the HY form the size distribution is around 15 Å with about 75% of the particles below 20 Å (Pd/HY, $d_{TEM} = 19$ Å). This is coherent with the formation of clusters in supercages with little lattice deformation. Some particles greater than 40 Å are nevertheless present, probably because of lattice defects created during NH_4(Na)Y treatment.

The two histograms and average sizes obtained for samples with additional treatment (Pd/NaYt, $d_{TEM} = 42$ Å, and Pd/HYt, $d_{TEM} = 18$ Å) are similar to the histograms of Pd/NaY and Pd/HY, suggesting that the particle size is little affected by this treatment. Nevertheless, direct observation of all samples reveals the presence of large particles on the external surface of zeolite crystallites only for Pd/NaYt. The real average size of this sample could be larger than that determined by the microtome method.

2.3. Xenon Measurements. Xenon adsorption isotherms and xenon chemical shift curves are plotted on Figures 5 and 6 for both zeolites. Spectra of xenon adsorbed in NaY and HY consist of single lines whose chemical shifts, δ_{NaY} and δ_{HY}, increase linearly with the number, N_{xe}, of adsorbed xenon atoms per gram of framework (Figures 5a and 6a). The values obtained by extrapolation of these lines to zero concentration are $\delta_{NaY} = 58$ ppm and $\delta_{HY} = 75$ ppm. The latter value is higher than expected, since it is known that the xenon chemical shift is very slightly modified by the replacement of Na^+ by H^+ ion. Therefore, as in TEM measurements, it seems likely

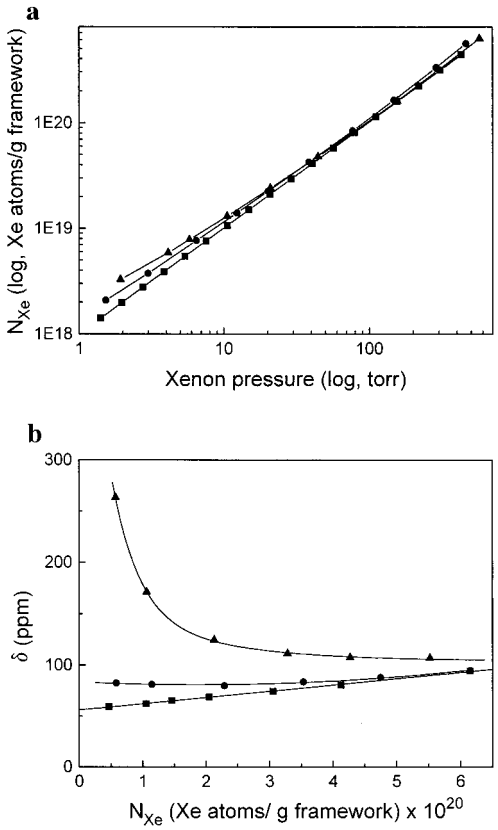

Figure 5. Xenon adsorption isotherms (a) and xenon chemical shift (b) of NaY (■), Pd/NaY (●), and Pd/NaYt (▲) samples at RT.

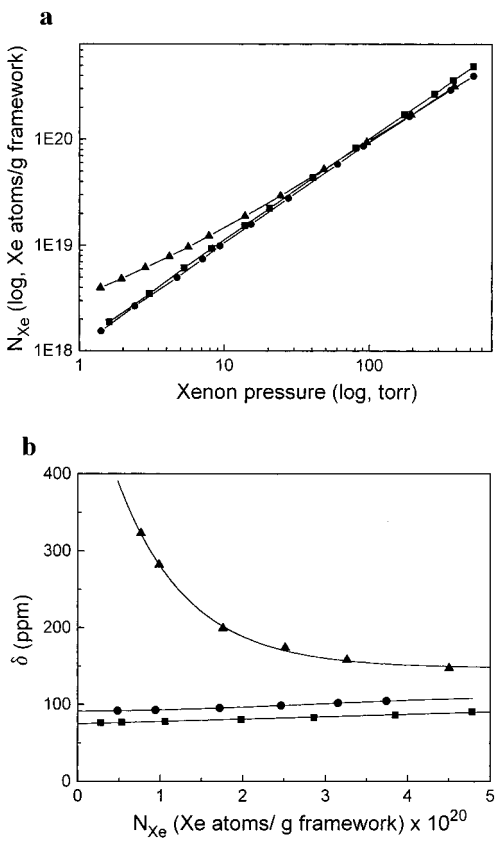

Figure 6. Xenon adsorption isotherms (a) and xenon chemical shift (b) of HY (■), Pd/HY (●), and Pd/HYt (▲) samples at RT.

that there are lattice defects (gaps and obstructions) in the HY form, probably caused by the thermal treatment of NH_4(Na)Y, which modifies xenon diffusion in the crystallites.

Before explaining the results obtained for metallic samples, let us recall some general considerations about chemical shift variations on metal/zeolite systems. The variation of the chemical shift of xenon (δ) adsorbed on metal/zeolite systems is usually explained by using a fast site-exchange model and can be written:

$$\delta = \delta_{ref} + f_s\delta_{s-Xe} + f_w\delta_{w-Xe} + \delta_{Xe-Xe} \quad \text{(ref 14)}$$

where f_s and δ_{s-Xe} or f_w and δ_{w-Xe} represent the mole fractions and the chemical shift of xenon adsorbed on strong or weak adsorption sites, respectively. Palladium clusters inside the zeolite are the strong adsorption sites, while Na^+, H^+ and aluminosilicate framework surface are the weak adsorption sites. δ_{Xe-Xe} expresses the influence of the xenon−xenon interactions. At low pressures, xenon is mainly adsorbed on the strong adsorption sites; this leads to a strong polarization and consequently a high chemical shift. When the xenon pressure increases, δ is averaged because of rapid exchange between strong and weak adsorption sites and, therefore, decreases. Finally, at high xenon pressures the xenon−xenon interactions become more important and δ increases linearly as for Y zeolites without metal. The reference δ_{ref} is the chemical shift of gas xenon extrapolated to zero pressure.

Isotherms of xenon adsorption (Figures 5a and 6a) establish that more xenon is adsorbed at low pressures for Pd/HYt and Pd/NaYt than for Pd/HY, Pd/NaY, and zeolites without metal. Therefore, we conclude that there are strong adsorption sites in Pd/HYt and Pd/NaYt samples. These strong adsorption sites are palladium clusters. For all samples, the xenon-adsorbed spectra consist of a single line. Only Pd/NaYt and Pd/HYt samples which have been treated with dioxygen and then dihydrogen present a variation of δ similar to that of metal-loaded zeolites, described previously, which confirms the presence of strong adsorption sites in the zeolite cavities. On the other hand, δ of Pd/HY sample (Figure 6b) increases linearly with N_{Xe}, which is a behavior similar to that of HY zeolite. In the case of Pd/NaY we observed a very slight decrease before the linear increase with xenon concentration (Figure 5b).

These results show that strong adsorption sites are detected by xenon only after dioxygen/dihydrogen treatment. To explain this phenomenon let us examine three hypotheses: first, there are metallic clusters inside the NaY and HY frameworks only after additional treatment; second, particles are located only inside sodalite cavities, where they are inaccessible to xenon; finally, particles are inside supercages but are hidden by ligand residues. The first hypothesis is easily excluded since TEM shows particles on all sectioned samples. Moreover, clusters obtained directly by heating in inert gas are really metallic, as confirmed by the *in situ* EXAFS experiments. We also exclude the presence of particles only inside sodalite cavities because $[Pd(en)]^{2+}$, which is too big (≈4.5 Å) to enter sodalite cages (window aperture 2.2 Å), was not heated under dioxygen before reduction. Then, during the reduction step particles were formed mainly in the supercages, as confirmed by the particle size (Table 2). Therefore, we conclude that residues of ethylenediamine prevent adsorption of xenon on the metallic surface perhaps by blocking supercage windows or, far more probably, by covering the particles. Treatment with O_2 for 12 h at 573 K removes organic compounds and allows the strong interaction of xenon with palladium atoms.

The difference observed between the δ variation curves of Pd/HY and HY (Figure 6b) is explained by the decrease in the pore volume of Pd/HY due to palladium clusters and organic residues inside the zeolite. This is the same explanation as for Pd/NaY and NaY (Figure 5b) but the difference is smaller since the particles are less numerous. The slight decrease in δ for low N_{Xe} on Pd/NaY is related to the presence of some "bare" palladium clusters, which is not observed for Pd/HY, probably because there are more residues.

TABLE 2: TEM, H_2 Chemisorption, EXAFS, and ^{129}Xe NMR Main Results from Pd/NaY, Pd/NaYt, Pd/HY, and Pd/HYt Samples

		H_2 chemisorption		EXAFS		
sample	TEM d_{TEM} (Å)	D	d_{H_2} (Å)[b]	CN	d_{EXAFS} (Å)[b]	^{129}Xe NMR δ (ppm)[c]
Pd/NaY	46	0.162	∼80			76
Pd/NaYt	42[a]	0.216	∼60	10.2−10.9	25−36	175
Pd/HY	19	0.118	>100			92
Pd/HYt	18	0.202	65−70	9.2−9.7	16−20	280

[a] Some large particles were observed by direct observation but not considered to determine d_{TEM}. [b] Assuming fcc cubo-octahedron shape (Figure 3). Range of incertitude is determined by assuming that CN of completely reduced Pd clusters are between PdPd and PdPd + PdO number. [c] For $N_{Xe} = 1 \times 10^{20}$ xenon atoms adsorbed/g of framework.

Since Pd/NaYt and Pd/HYt (without residues) have the same amount of palladium, it is interesting to compare their xenon chemical shifts. For example, when $N_{Xe} = 10^{20}$ the chemical shifts are 175 and 280 ppm on Pd/NaYt and Pd/HYt, respectively. These values are listed in Table 2 with the results of other techniques and confirm that the palladium dispersion is better on HY zeolite.

2.4. Hydrogen Chemisorption. Palladium dispersions obtained by hydrogen chemisorption (Table 2) are 0.16 and 0.12 for Pd/NaY and Pd/HY, respectively; therefore d_{H_2} calculated using the particle model (Figure 3) disagrees completely with d_{TEM}. Analysis of the ^{129}Xe NMR results in the previous section showed that hydrogen chemisorption is not a suitable method for determining the exposed surface of Pd/NaY and Pd/HY samples, since there are carbon and nitrogen residues in the vicinity of the palladium clusters. Nevertheless, as the dihydrogen molecule is smaller than the xenon atom and can reach the palladium surface easier, it is possible to detect a small amount of strongly adsorbed hydrogen.

On the Pd/NaYt sample, the amount of chemisorbed hydrogen leads to an average size around 60 Å ($D = 0.22$) which is coherent with d_{TEM} ($d_{TEM} = 42$ Å) especially if we consider that direct observation by TEM revealed large particles outside the zeolite framework. On the contrary, the dispersion ($D = 0.20$) and particle size ($d_{H_2} = 65-70$ Å) calculated for Pd/HYt disagree completely with the TEM ($d_{TEM} = 18$ Å) and ^{129}Xe NMR results. This point and the influence of zeolite acidity on palladium dispersion will be discussed later.

2.5. EXAFS Characterization of Pd/NaYt and Pd/HYt Samples. In order to clarify the results concerning the average particle size in the Pd/HYt sample, EXAFS measurements were carried out on this and on Pd/NaYt. To avoid modification of palladium cluster sizes, we recorded the EXAFS spectra on the two samples stored in air without additional treatment.

The $\chi(k)$ curve obtained after inverse FT on the region $R = 1.17-3.37$ Å of the experimental radial structure function is given in Figure 7a for the Pd/NaYt sample. The best fitted curve is also plotted. The corresponding Fourier transform and its best fit are represented in Figure 7b. In the same way, the Fourier-filtered EXAFS spectrum, corresponding to the Fourier transform, and the best fit for the Pd/HYt sample are plotted on Figure 8, a and b. The Fourier transforms of Fourier-filtered $\chi(k)$ show there are light atoms (between 1.5 and 2 Å) in the first coordination shell of Pd for both samples. Since Pd atoms of the metallic surface can adsorb O_2 at RT, oxygen in the first

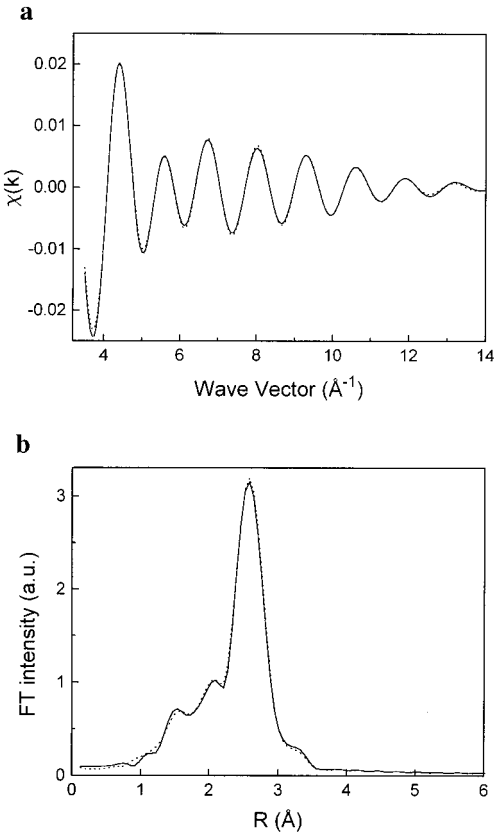

Figure 7. (a) Fourier-filtered EXAFS spectrum on $R = 1.17-3.37$ Å (—) and best fit curve (···) of Pd/NaYt; (b) corresponding Fourier transform (—) and best fit (···).

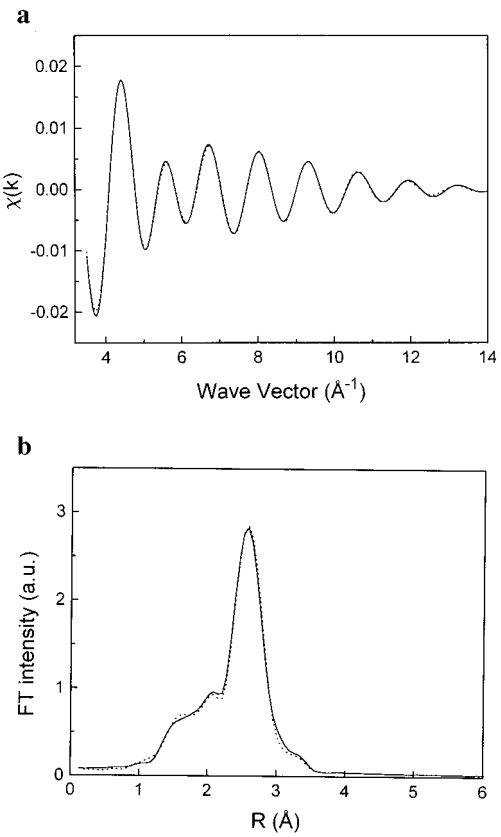

Figure 8. (a) Fourier-filtered EXAFS spectrum on $R = 1.17-3.37$ Å (—) and best fit curve (···) of Pd/HYt; (b) corresponding Fourier transform (—) and best fit (···).

coordination shell was taken into account in fitting calculated to experimental curves. Theoretical $\chi(k)$ and Fourier transform curves are very close to the experimental data. Therefore, the difference between the two samples can be discussed.

TABLE 3: EXAFS Results for Sample Pd/NaYt and Pd/HYt Stored in Air

	PdPd pair		PdO pair		
sample	*N*	*R* (Å)	*N*	*R* (Å)	CN
Pd/NaYt	10.2	2.741	0.7	1.969	10.9
Pd/HYt	9.2	2.736	0.5	1.993	9.7

Results for the fitting of the first coordination shell of palladium are reported in Table 3. Since the average coordination numbers of Pd/NaYt (CN = 10.9) and Pd/HYt (CN = 9.7) are lower than that of palladium foil (CN = 12), we may assume that palladium is in nanoparticle form. Moreover, Pd−Pd bond distances obtained from the EXAFS analysis are slightly shorter (2.741 Å for Pd/NaYt; 2.736 Å for Pd/HYt) than the usual value for palladium foil (2.76 Å). Many EXAFS studies have shown that the lattice parameter of supported metals is lower than in bulk metal,[21] and this is attributed to the formation of nanometer particles.

We tried to determine the average particle sizes of palladium clusters by using CN given in Table 3. Usually such a calculation makes sense only if the clusters are completely metallic. We considered that the number of O atoms in the first coordination shell of Pd is low enough to consider the CN of these palladium clusters without adsorbed oxygen to be taken as lying between the numbers for PdPd and PdPd + PdO. Average particle sizes (d_{EXAFS}) determined assuming this reflection and using fcc cubo-octahedron shape (Figure 3) are given in Table 2. Values obtained are $d_{EXAFS} = 25-36$ Å and $d_{EXAFS} = 16-20$ Å for Pd/NaYt and Pd/HYt, respectively. First, the d_{EXAFS} values are near d_{TEM} (42 Å for Pd/NaYt; 18 Å for Pd/HYt) and confirm also the difference between these two samples observed by ^{129}Xe NMR spectroscopy . Second, the d_{EXAFS} result for the Pd/HYt sample confirms that the H_2 chemisorption result ($D = 0.20$; $d_{H_2} = 65-70$ Å) is surprising.

In conclusion, CN and therefore particle sizes determined for samples without organic residues agree with the results of TEM, ^{129}Xe NMR, and xenon adsorption. These results establish that palladium is better dispersed on HY zeolite after removing carbon and nitrogen compounds than on NaY. The explanation of this and the conflicting data obtained from H_2 measurements will now be discussed.

2.6. Influence of Protons on Pd/HY Systems. We shall now discuss the dramatic influence of zeolite acidity on palladium cluster size and the divergence between the hydrogen chemisorption results and those of the other techniques. In work on the autoreduction of $[Au(en)_2]^{3+}$ on Y zeolites[10] we reported difficulties in preparing small gold particles on NaY, and we already found that H(Na)Y gave better results for the dispersion and thermal stability of gold. In the present work, autoreduction of $[Pd(en)]^{2+}$ leads also to better dispersion and stability on acidic Y zeolite. To explain this, let us consider the hypothesis of chemical anchorage proposed by Sachtler,[22,23] recently confirmed by theoretical calculation.[24] After the usual calcination/reduction process for preparing palladium particles in NaY zeolite, bare Pd^{2+} ions obtained are mainly in sodalite cages. The reduction step leads to proton formation in sodalites cages and small palladium clusters in the supercages. These clusters grow easily on heating. In the case of CaY or MgY, bare Pd^{2+} stay inside the supercages after calcination because Mg^{2+} and Ca^{2+}, which are better coordinated in small cages, preferentially occupy the sodalite cages. Therefore, reduction leads to protons and palladium clusters in the same cages, which may produce very stable particles. According to Sachtler, this phenomenon

is based on the formation of proton bridges ($O\cdots H\cdots M_m$ bonds) and results in positively charged clusters.

Let us consider our preparation method: $[Pd(en)]^{2+}$ complexes are located only in supercages before reduction. After autoreduction, the state of the oxidized ethylenediamine ligand is unknown, but if H^+ ions are formed, they are probably neutralized by the amine in the same way that NH_3 neutralizes H^+ generated during the reduction of Rh^{3+} on NaY zeolite.[25] Therefore, we may assume that H^+ ions are absent from the supercages of the Pd/NaY sample. On the HY form, Pd(0) obtained after autoreduction and zeolite counter-H^+ are in the same cages; chemical anchoring is then possible, which could explain the formation of highly dispersed and stable palladium clusters prepared on HY zeolite by our method. Recently, Xu *et al.*[26] observed by EXAFS that palladium clusters on HY zeolite are smaller than those prepared on Pd/NaY using the conventional calcination/reduction procedure. They also noted that the hydrogen chemisorption capacity of the Pd/HY catalyst was lower than that of Pd/NaY. According to these authors, palladium clusters in contact with protons (formation of $[Pd_n\text{-}H_x]^{x+}$ adduct) are responsible for the chemical anchoring and the marked decrease in hydrogen adsorption capacity (hydrogen suppression). Evidence by other authors also shows that strong adsorption of hydrogen on zeolite-encaged nickel[27] and ruthenium[28] particles is reduced in the presence of a high proton concentration. In this last work, Wang *et al.* established that hydrogen suppression decreases with increasing Si/Al ratio, *i.e.* with increasing acidity.

Conclusions

Direct reduction of Pd(II) to Pd(0) by ethylenediamine at 523 K using $[Pd(en)]^{2+}$ exchanged in Y zeolites appears to be a new method for obtaining thermally stable nanoparticles of palladium inside zeolite supercages. The autoreduction of $[Pd(en)]^{2+}$ was demonstrated by *in situ* EXAFS at the Pd K edge. ^{129}Xe NMR spectroscopy and xenon adsorption isotherms reveal that after reduction palladium particles are surrounded by organic residues which can be removed by treatment with dioxygen at 573 K.

Characterization by ^{129}Xe NMR, xenon adsorption, TEM, and EXAFS shows that palladium clusters are better dispersed on HY than NaY zeolite. Moreover, on the acidic zeolite, the particle size is not affected by additional treatment, contrary to those on NaY, for which TEM shows growth on the external surface of the zeolite crystallites. We established that the usual H_2 chemisorption technique is not suitable for determining the exposed surface of palladium clusters of reduced samples, because of surface coverage by organic residues. On the other hand, for a HY sample without residues, hydrogen chemisorption reveals a phenomenon of hydrogen suppression on Pd clusters.

According to work by Sachtler *et al.* on palladium chemical anchoring on acid zeolites, better dispersion, stability, and hydrogen suppression obtained in the present study on HY are related to palladium clusters in contact with protons inside the zeolite supercages. These results confirm an earlier study[10] on the formation of highly dispersed gold particles on H(Na)Y by the same autoreduction procedure.

Acknowledgment. The authors are indebted to Mr. Lavergne (Paris VI, France) for the excellent TEM negatives used for histograms and average size determinations.

References and Notes

(1) Delafosse, D. *J. Chem. Phys.* **1986**, *83*, 197.
(2) Maxwell, I. E. *Catal. Today* **1987**, *1*, 385.
(3) McCabe, R. W.; Usmen, R. K. In *Studies in Surface Science and Catalysis*; Hightower, J. W., Delgass, W. N., Iglesia, E., Bell, A. T., Eds.; 11th International Congress on Catalysis, Baltimore; Elsevier Science: Amsterdam, 1996; Vol. 101, p 355.
(4) Gallezot, P.; Alacron-Diaz, A.; Dalmon, J.-A.; Renouprez, A. J.; Imelik, B. *J. Catal.* **1975**, *39*, 334.
(5) Bergeret, G.; Gallezot, P.; Imelik, B. *J. Phys. Chem.* **1981**, *85*, 411.
(6) Homeyer, S. T.; Sheu, L. L.; Zhang, Z.; Sachtler, W. M. H.; Balse, V. R.; Dumesic, J. A. *Appl. Catal.* **1990**, *64*, 225.
(7) Zhang, Z.; Wong, T. T.; Sachtler, W. M. H. *J. Catal.* **1991**, *128*, 13.
(8) Tanabe, S.; Matsumoto, H.; Mizushima, T., Okitsu, K.; Maeda, Y. *Chem. Lett.* **1996**, *4*, 327.
(9) Sordelli, L.; Martra, G.; Psaro, R.; Dossi, C.; Coluccia, S. *J. Chem. Soc., Dalton Trans.* **1996**, *5*, 765.
(10) Guillemot, D.; Polisset-Thfoin, M.; Fraissard, J. *Catal. Lett.* **1996**, *41*, 143.
(11) Ito, T.; Fraissard, J. In *Proceedings of the 5th International Conference on Zeolites, Naples, Italy, 1980*; Rees, L. V., Ed.; Heyden: London, 1980; p 510.
(12) Moretti, G.; Sachtler, W. M. H. *Catal. Lett.* **1993**, *17*, 285.
(13) Pak, C.; Cho, S. J.; Lee, J. Y.; Ryoo, R. *J. Catal.* **1994**, *149*, 61.
(14) Pak, C.; Ryoo, R. *Appl. Magn. Reson.* **1995**, 8, 475, and references therein.
(15) Bonnin, D.; Kaiser, P.; Desbarres, J. Presented at Europhysics School on Chemical Physics: X-Ray Absorption, 1992.
(16) Polisset, M.; Fraissard, J. *Colloids Surf. A: Physicochem. Eng. Aspects* **1993**, *72*, 197.
(17) O'Rear, D. J.; Loffler, D. G.; Boudart, M. *J. Catal.* **1990**, *121*, 131.
(18) I'ball, J.; Macdougall, M.; Scrimgeour, S. *Acta. Crystalallogr. Sect. B.* **1975**, *31*, 1672.
(19) Van Hardeveld, R.; Hartog, F. *Surf. Sci.* **1969**, 15, 189.
(20) Jaeger, N. I.; Ryder, P.; Schulz-Ekloff, G. In *Studies in Surface Science and Catalysis*; Jacobs, P. A., Jaeger, N. I., Jiru, P., Kazansky, V. S., Schulz-Ekloff, G., Eds.; Structure and Reactivity of Modified Zeolites; Elsevier: Amsterdam, 1984; Vol. 18, p 299.
(21) Burch, R. In *Catalysis*; The Royal Society of Chemistry: London, 1986; Vol. 7, p 161, and references therein.
(22) Sheu, L. L.; Knozinger, H.; Sachtler, W. M. H. *J. Am. Chem. Soc.* **1989**, *111*, 8125.
(23) Sachtler, W. M. H.; Stakheev, A. Y. *Catal. Today* **1992**, *12*, 283, and references therein.
(24) Yakovlev, A. L.; Zhidomirov, G. M.; Neyman, K. M.; Nasluzov, V. A.; Rosch, N. *Ber. Bunsenges. Phys. Chem.* **1996**, *100*, 413.
(25) Wong, T.; Zhang, Z.; Sachtler, W. M. H. *Catal. Lett.* **1990**, *4*, 365.
(26) Xu, L.; Zhang, Z.; Sachtler, W. M. H. *J. Chem. Soc., Faraday Trans.* **1992**, *88* (15), 2291.
(27) Suzuki, M.; Tsutsumi, K.; Takahashi, H. *Zeolites* **1982**, *1*, 193. Suzuki, M.; Tsutsumi, K.; Takahashi, H. *Zeolites* **1982**, *2*, 185.
(28) Wang, H-T.; Chen, Y. W.; Goodwin, J. G. *Zeolites* **1984**, *4*, 56.